Small-Angle Neutron Scattering Investigations of Layer−Block Dendrimers in Aqueous Solutions

Katsuya Funayama,[†] Toyoko Imae,*[,†,‡] Keigo Aoi,[§] Kaname Tsutsumiuchi,[§] Masahiko Okada,[§] Michihiro Furusaka,[||] and Michihiro Nagao[⊥]

Graduate School of Science and Research Center for Materials Science, Nagoya University, Chikusa, Nagoya 464-8602, Japan, Graduate School of Bioagricultural Sciences, Nagoya University, Chikusa, Nagoya 464-8601, Japan, Institute of Materials Structure Science, High Energy Accelerator Research Organization, Tsukuba 305-0801, Japan, and Institute for Solid State Physics, The University of Tokyo, Tokai 319-1106, Japan

Received: September 11, 2002; In Final Form: November 25, 2002

Structures of poly(trimethyleneimine)/mono(amido amine) dendrimer with hydroxyl end groups and poly(amido amine) dendrimer with galactose having glycopeptide end groups were characterized in aqueous solutions and compared with that of poly(amido amine) dendrimer with hydroxyl end groups reported before (*Langmuir* **1999**, *15*, 4076). External contrast variation results of small-angle neutron scattering suggested the segment density distribution in dendrimer. The segment density distribution and solvent penetration amount in the fifth generation dendrimers were evaluated on the basis of the five concentric layers model. Those differed among three dendrimers, depending on the hydrophilic or hydrophobic interior segment and the small or bulky terminal group. Moreover, the profile of segment density distribution is not necessarily consistent with that of solvent penetration amount.

Introduction

Dendrimers, which are three-dimensional highly branched polymers, have been paid attention to as a novel class of macromolecules.[1,2] Numerous efforts have been made for the developments not only on the synthesis of dendrimers but also on its characterization and theoretical analysis. The structural concept of the dendrimer might be compared with that of globular polymers, like proteins and spherical self-assemblies, such as micelles and vesicles. From this viewpoint, a great deal of potential for industrial and medical applications is expected for dendrimers, as well as the analogous materials described above. Specific knowledge of the free void in dendrimers is required for different uses of the dendrimers, such as for the controlled host of drug molecules.

Small-angle neutron scattering (SANS) is very useful as a tool for analyzing experimentally the nanometer structure. Almost all of the studies performed by SANS in dendrimers were concerned with the conformational analysis of dendrimers in solution, to confirm the free void. Bauer et al.[3] characterized the sizes of poly(amido amine) (PAMAM) dendrimers in D_2O and methanol-d_4. Briber et al.[4] studied the effects of acid or salt on the interactions between PAMAM dendrimers in D_2O. Scherrenberg et al.[5] investigated the molecular characteristics of poly(propyleneimine) dendrimers with two different types of end groups. The structural investigation of poly(trimethyleneimine) (PTMIN) dendrimers in D_2O as a function of concentration and acidity was carried out by Ramzi et al.[6] Stark et al.[7] discussed the segmental dynamics in carbosilane dendrimers with perfluorinated end groups using quasielastic neutron scattering. Nisato et al.[8,9] examined the structure of ionic PAMAM dendrimers in D_2O and analyzed quantitatively the swelling response of the dendrimer, which is affected by the charges in solution conditions. Evmenenko et al.[10] measured the size of poly(benzyl ether) dendrimers with different molecular architectures. They found that the effect of solvent type (polar and nonpolar organic solvents) on dendrimer size was minimal.

SANS investigations using the external contrast variation technique were performed by Pötschke et al.[11] for PTMIN dendrimers with hydrophobic end groups in mixed solvents of protonated and deuterated dimethylacetamide. The contrast variation technique was also applied by us[12] to the structural analysis of PAMAM dendrimers with hydroxyl end groups in mixed D_2O-H_2O solvents. Topp et al.[13] discussed the spatial distribution of the terminal groups of PAMAM dendrimers, which have partially deuterated unities, by the internal contrast variation.

The theoretical approach to the dendritic structure was carried out side by side with the experimental ones. The prediction of a limit for the divergent dendritic growth of dendrimers was made by de Gennes and Hervet.[14] Naylor et al.[15] predicted a dramatic change in morphology with the generation of dendrimers by means of the molecular dynamics simulations. From a kinetic growth study of starburst molecules by Lescanec and Muthukumar,[16] the end groups at a given generation were reported to be not on the surface but buried within the molecule. A self-consistent mean field approximation, carried out by Boris and Rubinstein,[17] predicted that the segment density decreases monotonically from the center of the starburst dendrimer. Welch and Muthukumar[18] demonstrated that the intramolecular density profile of dendritic polyelectrolytes in solution could be tailored by varying the ionic strength of the solvent. Lue[19] investigated the effect of hyperbranching on the structure of dendritic polymer and the thermodynamics in solutions by Monte Carlo

* To whom correspondence should be addressed. Tel: +81-52-789-5911. Fax: +81-52-789-5912. E-mail: imae@nano.chem.nagoya-u.ac.jp.
[†] Graduate School of Science, Nagoya University.
[‡] Research Center for Materials Science, Nagoya University.
[§] Graduate School of Bioagricultural Sciences, Nagoya University.
[||] High Energy Accelerator Research Organization.
[⊥] The University of Tokyo.

10.1021/jp026965h CCC: $25.00
Published on Web 01/22/2003

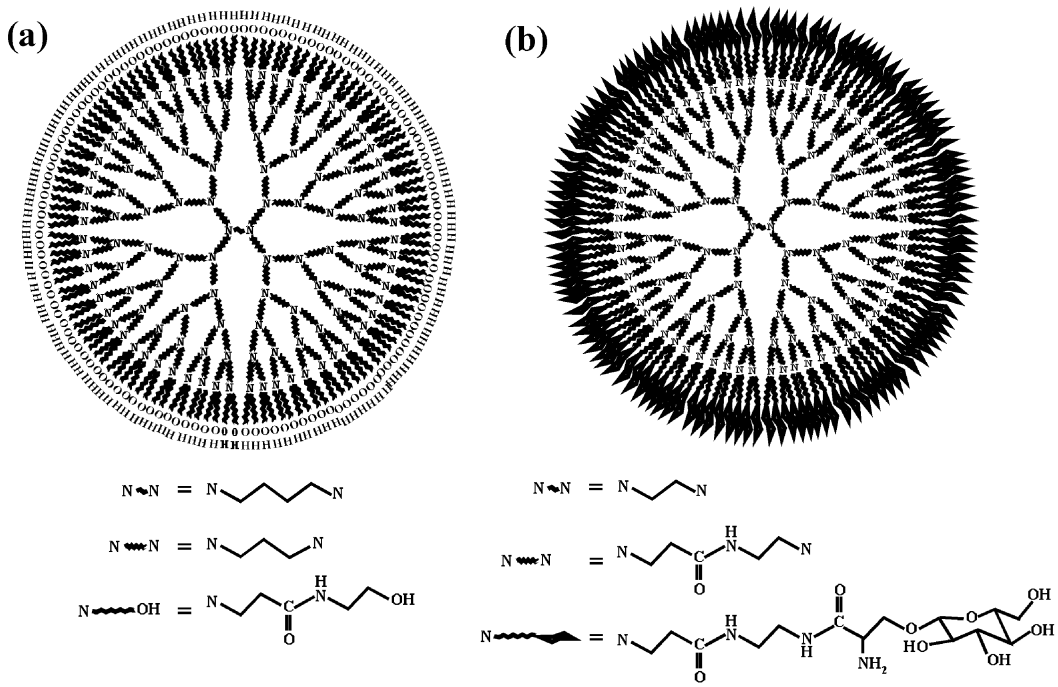

Figure 1. Chemical structures of G5 dendrimers. (a) OH type PTMIN/AMAM dendrimer; (b) sugar ball.

simulations. Ganazzoli et al.[20] evaluated the good solvent expansion of dendrimers by the self-consistent free energy minimization. Despite various reports, the structural discussion of dendrimers is not necessarily in a conclusive situation.

To clarify the morphological properties of dendrimers, one has to consider the relationship with the chemical structure of the dendrimer. We[12] investigated quantitatively the segment density of fifth generation (G5) PAMAM dendrimers with hydroxyl end groups (OH type PAMAM dendrimer) and the solvent penetration into the dendrimer. In the present work, two water soluble layer−block dendrimers, which can be compared with OH type PAMAM dendrimers, were prepared. One is the G5 poly(trimethyleneimine)/mono(amido amine) dendrimer with hydroxyl end groups (OH type PTMIN/AMAM dendrimer), as shown in Figure 1a. This dendrimer has a repeating unit of trimethyleneimine and a core unit of butylenediamine, which take more hydrophobic nature than amido-amine and ethylenediamine units in the OH type PAMAM dendrimer. Another is the G5 and G6 PAMAM dendrimers with galactose having glycopeptide end groups (sugar ball), as shown in Figure 1b. These end groups are different from hydroxyl groups with regards to the spatial conformation. The structural analysis of the two dendrimers in solution was performed by the external contrast variation technique of SANS, and the effect of the chemical structure of the internal and terminal units is discussed in comparison with the results of the OH type PAMAM dendrimer reported before.[12] The coherent scattering intensity of SANS depends on the difference between the scattering length densities of the solvent and the scatter. Therefore, using the external contrast variation method, one can obtain information of the density profile.

Experimental Section

Dendrimers. G5 OH type PTMIN/AMAM dendrimer was synthesized by the divergent route from G4 PTMIN dendrimer (butylenediamine core) with amine end groups.[1] The number of terminal hydroxyl groups and the molecular weight of OH type PTMIN/AMAM dendrimers are 128 and 26 000, respectively.

G5 and G6 sugar balls were prepared by the radial growth polymerization of sugar-substituted α-amino acid *N*-carboxyanhydrides with G5 and G6 PAMAM dendrimers (ethylenediamine core) with amine end groups, respectively.[21−23] The numbers of terminal hydroxyl groups of G5 and G6 sugar balls are 128 and 256, respectively, and their molecular weights are 60 000 and 122 000, respectively.

Distilled H_2O was repurified by Milli-Q. D_2O (99.75%) was purchased from Wako Pure Chemical Industries, Ltd.

Measurements. Microscopic observations were performed by a tapping mode atomic force microscopy (AFM) and a transmission electron microscopy (TEM) at room temperature. Cast specimens for the observations on Digital Instruments NanoScope III AFM and Hitachi H-800 TEM (operated at 100 kV) were prepared by depositing 1.0 wt % H_2O solutions of G5 dendrimers on the substrates, draining, and then drying in air. Freshly cleaved mica and carbon-coated grid were used as the substrates for AFM and TEM, respectively.

Size determinations of dendrimers were done, at 25 °C, on an Otsuka Electronics DLS-700 dynamic light scattering (DLS) spectrometer, equipped with an Ar ion laser (488 nm) and an ALV-5000 correlation function analyzer. The concentration of the dendrimer in H_2O and the measured scattering angle were 1.0 wt % and 90°, respectively.

SANS measurements were carried out using the cold neutron small-angle scattering instrument WINK at the High Energy Accelerator Research Organization (KEK), Tukuba, Japan, and the SANS-U diffractometer (sample to detector distance: 1, 4, and 8 m) of JRR-3M, at the Japan Atomic Energy Research Institute (JAERI), Tokai, Japan. The neutron radiation wavelength on the WINK and SANS-U instruments was $\lambda = 1-16$ and 4−10 Å, respectively. The rectangular quartz cells used were of $22^{W} \times 40^{H} \times 2^{D}$ mm^3 for WINK and $10^{W} \times 40^{H} \times 2^{D}$ mm^3 for SANS-U. The raw data at radial distance were averaged to produce the SANS intensities *I(Q)* as a function of scattering vector amplitude *Q* of

$$Q = \frac{4\pi}{\lambda} \sin\left(\frac{\theta}{2}\right) \tag{1}$$

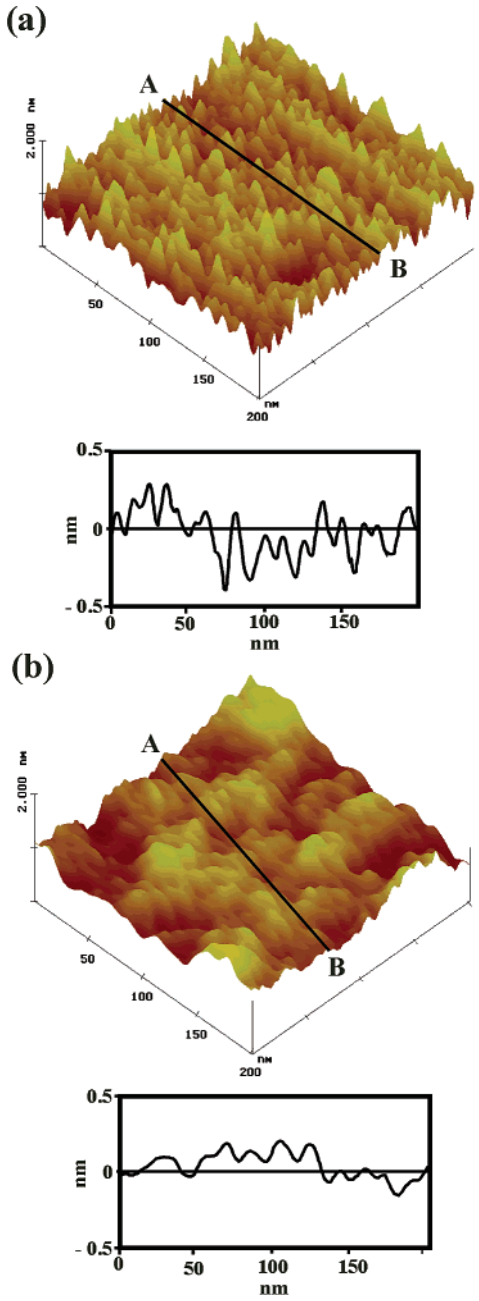

Figure 2. AFM images of G5 dendrimers deposited on mica from 1.0 wt % H_2O solutions. (a) OH type PTMIN/AMAM dendrimer; (b) sugar ball. Lower figures represent the cross-sectional profiles of AB lines shown in upper ones.

where θ is the scattering angle.[24−29] The background subtraction was carried out for a quartz cell and a solvent.[24,26,27] The incoherent contribution of the dendrimer molecules to the scattering intensity was evaluated at the high Q range and subtracted from the scattering data.[26,30] The resulting intensity from SANS-U was calibrated by a standard sample, luporen. The mixing ratio of solvent, D_2O-H_2O mixture, is denoted by % D_2O (= $D_2O/(D_2O + H_2O)$ v/v %).

Results

Microscopic Observation and Size Estimation. The AFM images shown in Figure 2 were obtained for the cast films prepared on mica from 1.0 wt % H_2O solutions of G5 dendrimers. Particles, associated with the dendrimer molecules, were observed in the images. The deposition films of dendrimers

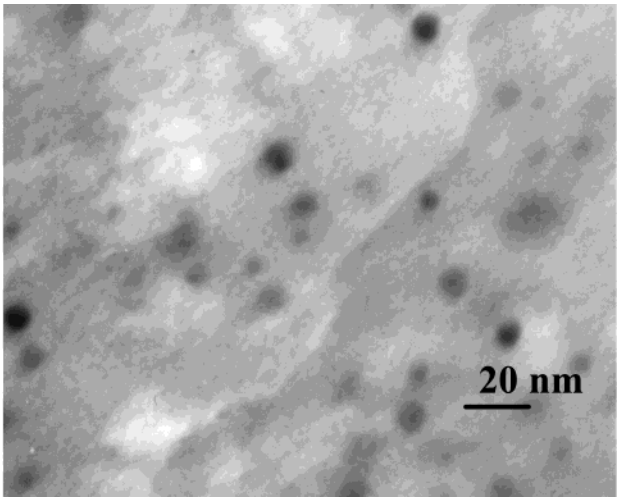

Figure 3. TEM photograph of G5 sugar balls deposited on a carbon grid from a 1.0 wt % H_2O solution.

displayed rather flat surfaces, and the surface height differences were only 3−4 Å for the OH type PTMIN/AMAM dendrimer and sugar ball. These results are similar to those observed for the G5 OH type PAMAM dendrimer.[12] It should be noticed that the deposition film surface of the sugar ball (Figure 2b) was slightly flatter than that of the OH type PTMIN/AMAM dendrimer (Figure 2a).

A TEM photograph in Figure 3 showed some G5 sugar ball molecules on a carbon grid. In comparison with an AFM result (Figure 2b) of G5 sugar ball deposited on mica substrate, it was obvious that the less adsorption of water soluble dendrimer, sugar ball, was affected by the hydrophobic surface of the substrate. The hydrodynamic radius of G5 sugar balls in a 1.0 wt % H_2O solution was determined to be 54 Å by DLS. This value is equivalent to that obtained from TEM. On the other hand, in the case of G5 OH type PTMIN/AMAM dendrimer in a 1.0 wt % H_2O solution, the scattering intensity was so weak that the size could not be determined by DLS.

SANS. Figure 4 shows double logarithmic plots of the SANS intensity $I(Q)$ vs the scattering vector amplitude Q for dendrimers in 100, 90, 75, and 50% D_2O. The Q dependence of SANS intensities for the G5 OH type PTMIN/AMAM dendrimer solutions was remarkable at 100% D_2O and became dull with decreasing D_2O content, as it can be seen in Figure 4a. Similar behavior was observed on SANS results for the G5 OH type PAMAM dendrimer solutions.[12] On the other hand, SANS profiles for the G5 and G6 sugar ball solutions, as seen in Figure 4b,c, were less influenced by the content of D_2O. That may have originated from density distribution inside dendrimer molecules.

For monodisperse particles, the SANS intensity $I(Q)$ as a function of Q can be written as[24−29]

$$I(Q) = n_p P(Q) S(Q) \tag{2}$$

where n_p is the number density of particles, $P(Q)$ is the intraparticle form factor, which depends on the particle geometry, and $S(Q)$ is the interparticle structure factor. For dilute solutions of nonionic dendrimers, as it is the case in the present work, $S(Q)$ approaches unity. For homogeneous particles such as dendrimers, if $QR_G \ll 1$, the radius of gyration R_G can be evaluated from the Guinier equation

$$P(Q) = V^2(\rho - \rho_S)^2 \exp\left(-\frac{R_G{}^2 Q^2}{3}\right) \tag{3}$$

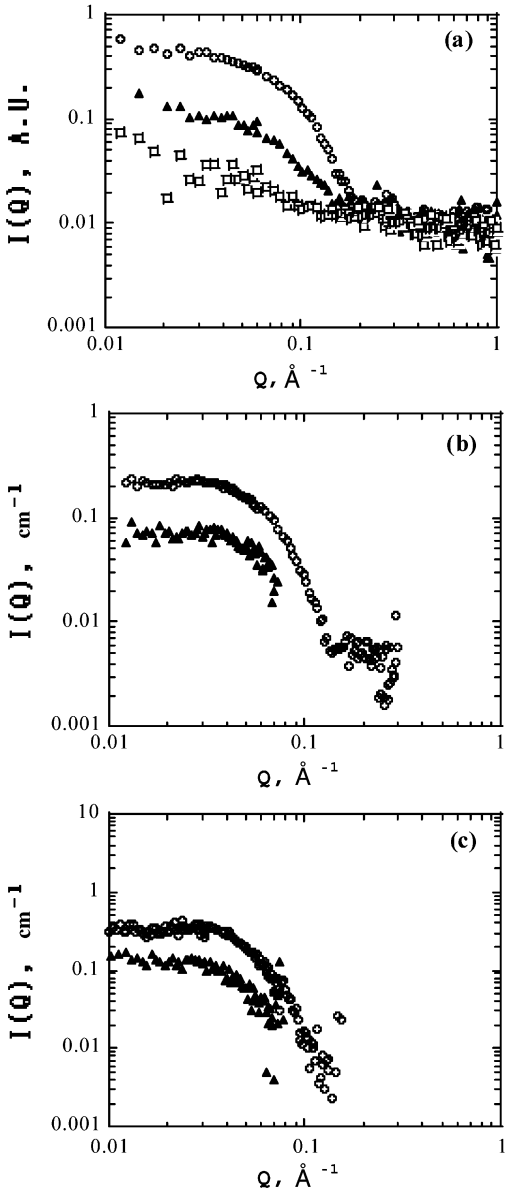

Figure 4. Double logarithmic plots of SANS intensity $I(Q)$ vs scattering vector Q for 1.0 wt % solutions of dendrimers at different solvent mixing ratios of D_2O-H_2O mixtures. (a) G5 OH type PTMIN/AMAM dendrimer; (b) G5 sugar ball; (c) G6 sugar ball. % D_2O: ○, 100; ▲, 75; □, 50.

where V is a total volume of the particle and ρ and ρ_S are the mean coherent neutron scattering length densities of the particle and the solvent, respectively. The external contrast variation is performed by varying the mean coherent neutron scattering length density of the solvent.[26,27,29] Then

$$\rho_S = \alpha\rho_D + (1 - \alpha)\rho_H \quad (4)$$

where α is the fractional number of D_2O molecules in the mixed solvent, that is, % D_2O, and ρ_D and ρ_H are the mean coherent neutron scattering length densities of D_2O and H_2O, respectively.

The apparent R_G values evaluated from the Guinier equation are plotted as a function of % D_2O in Figure 5, where those previously reported for the G5 OH type PAMAM dendrimer[12] are also included. The Guinier fittings were done using the least-squares fit for the Guinier region of $q = 0.03-0.1$ Å^{-1}. The cc values for fitting were 0.99, 0.93−0.95, and 0.80 for D_2O % = 90−100, 65−75, and 50%. From eqs 3 and 4, the variation of

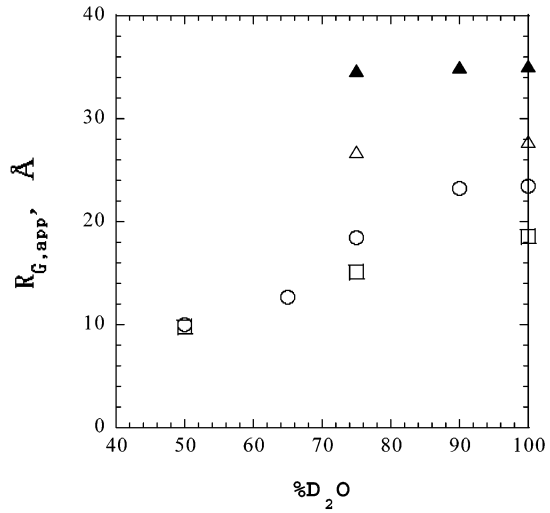

Figure 5. Apparent radii of gyration $R_{G,app}$ as a function of % D_2O for 1.0 wt % solutions of dendrimers. □, G5 OH type PTMIN/AMAM dendrimer; △, G5 sugar ball; ○, G5 OH type PAMAM dendrimer (ref 12).

TABLE 1: Size of G5 Dendrimers Obtained from SANS, DLS, and AFM Measurements

dendrimer	R_G[a] (Å)	R_{SANS}[b] (Å)	R_H[c] (Å)	R_{AFM}[d] (Å)	R_{cpk}[e] (Å)	R_5[f] (Å)
PTMIN/AMAM dendrimer	19	24		25	20−28	24
sugar ball	29	37	54	50	26−53	31
OH PAMAM dendrimer[g]	23	30	39	39	22−43	26

[a] Radius of gyration obtained from the Guinier region for SANS of a D_2O solution. [b] Radius calculated from the equation $R_{SANS}^2 = 5/3R_G^2$ for a hard sphere model. [c] Hydrodynamic radius obtained from DLS. [d] Radius obtained from AFM images. [e] Radius calculated from a CPK model for contracted to extended structures. [f] Radius obtained from the theoretical calculation of a five layers model. [g] Ref 12.

% D_2O is expected to affect only the absolute values of $P(Q)$ but not its profiles or the absolute values of R_G. This is the case for the G5 sugar ball, for which the size was almost independent of % D_2O. However, for the G5 OH type PTMIN/AMAM dendrimer, the R_G decreased remarkably with decreasing % D_2O. This behavior is similar to that of G5 OH type PAMAM dendrimer.[12] This indicates that the chemical structure of the interior or the exterior segment is related to the density distribution in the dendrimers.

Discussion

Dendrimers with different interior and exterior chemical structures showed different SANS results (Figure 4) and different dependence of R_G on % D_2O (Figure 5). (The dendrimer sizes are evaluated as the radii obtained from the scattering measurements and the microscopic observations.) For comparison purposes, the radius of gyration, calculated from the Guinier region of the SANS results for the D_2O solutions of dendrimers, was converted to a radius R_{SANS} by the relation $R_{SANS}^2 = 5/3R_G^2$ for a hard sphere model. These radii are listed in Table 1, where the hydrodynamic radius R_H measured by DLS and the radius R_{AFM} observed by AFM are also included. Data for the OH type PAMAM dendrimer[12] are also listed in Table 1. Each radius is within the possible size range calculated from the Corey−Pauling−Koltum (CPK) model.[1] In the case of the G5 sugar ball and the OH type PAMAM dendrimer, although the R_{AFM} and R_H are close to the R_{CPK} calculated for the more extended structure, the R_{SANS} is smaller. Lowering the neutron scattering length density difference between the

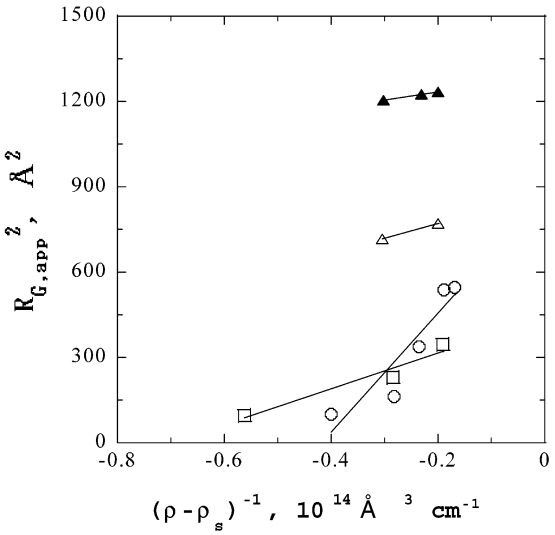

Figure 6. Mean square of $R_{G,app}$ plotted against the reciprocal of the contrast $\rho-\rho_s$ for 1.0 wt % solutions of dendrimers. □, G5 OH type PTMIN/AMAM dendrimer; △, G5 sugar ball; ○, G5 OH type PAMAM dendrimer (ref 12).

dendrimer and the solvent could cause this smaller R_{SANS} value. On the other hand, the R_{SANS} of the G5 OH type PTMIN/AMAM dendrimer is close to the R_{AFM}. These results indicate that the G5 OH type PTMIN/AMAM dendrimer has a different scattering length density profile than the sugar ball and the OH type PAMAM dendrimer.

The layer−block dendrimers in the present work were prepared through a divergent route, which introduces branching sites and spacers by repetitive reaction steps starting from a central core. The segment density in these dendrimers might, therefore, be different at each generation. To elucidate the segment density distribution in these dendrimers, the analysis by Stuhrmann et al.[31−33] was applied for the obtained SANS results. When the mean coherent neutron scattering length density ρ of the particle is defined as an average value of the local scattering length density $\rho(r)$ at the radial distance r from a particle center

$$\rho(r) = \rho + \Delta\rho(r) \tag{5}$$

$\Delta\rho(r)$ is a fluctuation of the density around the mean value and becomes zero by averaging over the volume V. From this definition, the radius of gyration R_G can be expressed as follows

$$R_G^2 = R_{GV}^2 + \left(\frac{V}{\rho - \rho_S}\right)\int_V \Delta\rho(r) r^2 d^3r \tag{6}$$

and

$$R_{GV} = \frac{1}{V}\int_V r^2 d^3r \tag{7}$$

Figure 6 shows plots of R_G^2 against the reciprocal of $(\rho - \rho_S)$. Positive slopes for the G5 OH type PTMIN/AMAM dendrimer and the G5 and G6 sugar balls were obtained as well as that for G5 OH type PAMAM dendrimer.[12] Positive values of $\int_V \Delta\rho(r) r^2 d^3r$ in eq 6 support the idea that there are segment density distributions in the dendrimers. Therefore, it is obvious that the mean coherent neutron scattering length density of the segments in the dendrimers has a remarkable distribution in addition to the distribution of the density of solvent penetrated into the dendrimer, as suggested in the case of the OH type PAMAM dendrimer.[12]

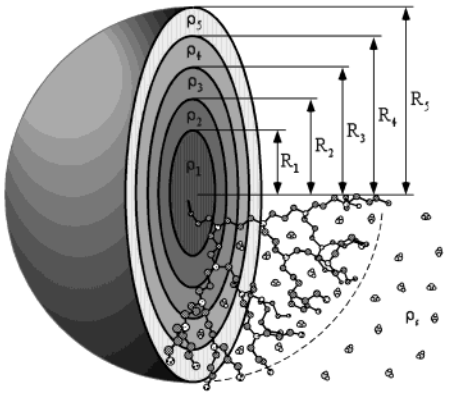

Figure 7. Geometric definition of a spherical "five layers model" consisting of a concentric structure applied for a G5 dendrimer in solution.

In the case of a hard sphere with a radius R, the intraparticle form factor $P(Q)$ is described by

$$P(Q) = \left\{\frac{4\pi R}{3}(\rho - \rho_S)\frac{3J_1(QR)}{QR}\right\}^2 \tag{8}$$

where $J_1(x) = (\sin x - x\cos x)/x^2$ is the first-order Bessel function.[24−29] Suppose that a spherical G5 dendrimer consists of five concentric layers, as depicted in Figure 7, since the dendrimer has the layer structure as mentioned above. Generations of the dendrimer are equalized to the layers with different mean density; each generation has a homogeneous mean density. Then, $P(Q)$ is the sum of the terms from a central core of radius R_1 and the surrounding shells with thickness of $R_i - R_{i-1}$, as defined by the expression[12,34]

$$P(Q) = \left\{\sum_{i=1}^{4}\frac{4\pi R_i}{3}(\rho_i - \rho_{i+1})\frac{3J_1(QR_i)}{QR_i} + \frac{4\pi R_{i=5}}{3}(\rho_{i=5} - \rho_S)\frac{3J_1(QR_{i=5})}{QR_{i=5}}\right\}^2 \tag{9}$$

where ρ_i is the mean coherent neutron scattering length density in the ith layer of the dendrimer. When the solvent penetrates into the dendrimers, the scattering length density in the ith layer must include the contribution of the dendrimer and the penetrated solvent, that is

$$\rho_i = \rho_{den,i} + A_i\rho_S \tag{10}$$

where $\rho_{den,i}$ is the mean coherent neutron scattering length density of dendrimer segment in the ith layer and A_i is the number density of the solvent in the ith layer.

When eqs 9 and 10 for the five layers model including the solvent penetration (Figure 8) are applied, better fit curves of the SANS results for the D_2O solutions of G5 dendrimers were obtained especially in the range up to $Q = 0.2$ Å^{-1}, where the calculations for a hard sphere model (eq 8) failed. The optimum parameters used for the calculations of SANS intensities are listed in Table 2 and compared with those for the OH type PAMAM dendrimer.[12] The radii R_5 of the fifth layer are also included in Table 1. It can be observed that for sugar balls and OH type PAMAM dendrimers, although the R_5 values are close to R_{SANS} and radii calculated by the CPK model, the values are smaller than R_H and R_{AFM}. Therefore, these dendrimer molecules have to be related to the solvent penetration into them.

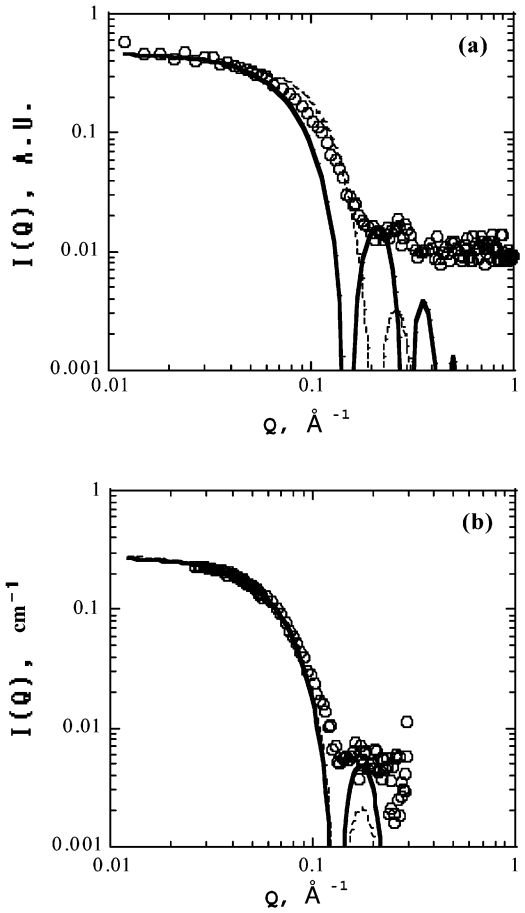

Figure 8. Double logarithmic SANS intensity profiles for 1.0 wt % D_2O solutions of G5 dendrimers. (a) OH type PTMIN/AMAM dendrimer; (b) sugar ball. ○, experimental data; broken line, the calculation from a hard sphere model; solid line, the calculation from a five layers model considering the solvent penetration into the dendrimer.

The obtained neutron scattering length density $\rho_{den,i}$ profiles are illustrated in Figure 9. With increasing the layer i, the segment scattering length density $\rho_{den,i}$ of the G5 OH type PTMIN/AMAM dendrimer increases, whereas that of the G5 sugar ball shows a minimum at $i = 4$. Both behaviors are different from that of the OH type PAMAM dendrimer, which presents both a minimum (for $i = 2$) and a maximum (for $i = 4$).[12] The difference should be because of the sizes of the central core, repeating unit, and terminal groups. The core structure of OH type PTMIN/AMAM dendrimers, growing from butylenediamine, has more space than those of sugar balls and OH type PAMAM dendrimers with an ethylenediamine central core. Sugar balls and OH type PAMAM dendrimers have a larger repeating unit than the OH type PTMIN/AMAM dendrimer, but terminal groups of sugar balls are larger than the others.

The difference observed for ρ_i values depends on the solvent penetration. Then, dendrimers show different profiles of solvent penetration, as can be seen in Table 2. The solvent penetration A_i of G5 OH type PTMIN/AMAM dendrimers is more poor in the interior layers than those of G5 sugar balls and OH type PAMAM dendrimers. This indicates that the trimethyleneimine repeating unit in OH type PTMIN/AMAM dendrimers is more hydrophobic than the amido-amine repeating unit in sugar balls and OH type PAMAM dendrimers. However, low or no solvent penetration was observed in the fifth layer of sugar balls, although the terminal groups in the fifth layer have more hydrophilic nature. For layer−block dendrimers with large terminal groups, the solvent penetration is restricted in the most exterior layer, which has the denser segment packing. Figure 10a shows the number of penetrated solvents per segment residue, A_i/segment, as a function of radial distance. In the interior layers, sugar balls and OH type PAMAM dendrimers displayed similar A_i/segment, 2−7, because of the same repeating unit. However, the values of A_i/segment for OH type PTMIN/AMAM dendrimers are only 1 in the interior layers and 2 in the fifth layer, which are always smaller than those observed in OH type PAMAM dendrimers, although both dendrimers have same terminal group.

TABLE 2: Parameters Obtained from SANS Calculations for 1.0 wt % D_2O Solutions of G5 Dendrimers

dendrimer		$i = 1$	$i = 2$	$i = 3$	$i = 4$	$i = 5$
OH type PTMIN/	R_i (Å)	10	13	16	19	24
AMAM	$\rho_{den,i}$ (10^{-14} cm Å^{-3})	0.2	0.2	0.3	0.4	0.7
dendrimer	ρ_i (10^{-14} cm Å^{-3})	0.7	0.8	1.0	1.2	2.1
	A_i	10	15	30	50	200
	A_i/segment	1	1	1	1	2
sugar ball	R_i (Å)	8	11	15	21	31
	$\rho_{den,i}$ (10^{-14} cm Å^{-3})	1.4	1.1	0.9	0.6	1.1
	ρ_i (10^{-14} cm Å^{-3})	2.8	3.9	4.7	4.2	1.1
	A_i	15	50	170	470	0
	A_i/segment	2	3	5	7	0
OH type	R_i (Å)	8	11	14	17	26
PAMAM	$\rho_{den,i}$ (10^{-14} cm Å^{-3})	1.4	1.1	1.3	1.7	0.4
dendrimer[a]	ρ_i (10^{-14} cm Å^{-3})	2.8	3.6	6.2	10	2.6
	A_i	15	50	150	400	620
	A_i/segment	2	3	5	6	5

[a] Ref 12.

The segment density was evaluated from the radius R_i and is plotted in Figure 10b as a function of the radial distance. The low segment density in the first layer of OH type PTMIN/AMAM dendrimers, different from that of the other dendrimers, is caused by the core structure, as mentioned above. The segment density of OH type PTMIN/AMAM dendrimers increases with increasing radial distance, but on the other hand, that of the sugar ball decreases with increasing the generation layer up to the fourth layer. In the case of OH type PTMIN/AMAM dendrimers, the growth of the generation leads to a dense segment packing. Sugar balls have the large glycopeptide terminal groups and then, the segments in the interior generation layers, like the third and fourth layers, are extended. The segment density of sugar balls, therefore, displays the opposite behavior to OH type PTMIN/AMAM dendrimers. Moreover, for both layer−block OH type PTMIN/AMAM dendrimers and sugar balls, the densities in the fifth layer are high because of the relatively large and extended terminal groups, respectively, as compared with those of the interior layers. These density profiles are different from the result obtained for the OH type PAMAM dendrimer, which has the same terminal group or the same repeating unit.[12]

The density profile of dendrimers derived theoretically by de Gennes and Hervet[14] is minimal at the center and increases toward the outer edge. This profile is consistent with the analytical result of the G5 OH type PTMIN/AMAM dendrimer in the present work. However, their theoretical prediction does not conform to the case of the sugar ball, which exhibits the maximum at the center. Lescanec and Muthukumar[16] reported by simulation of starburst molecules that there is a maximum of the density at the center of the molecule. Such a density profile was obtained from SANS for the dimethylacetamide solution of G5 PTMIN dendrimer with hydrophilic terminal groups.[11] The SANS study was used for probing the location of terminal groups of the dendrimer, and it was confirmed that the terminal groups of G7 PAMAM dendrimers were concen-

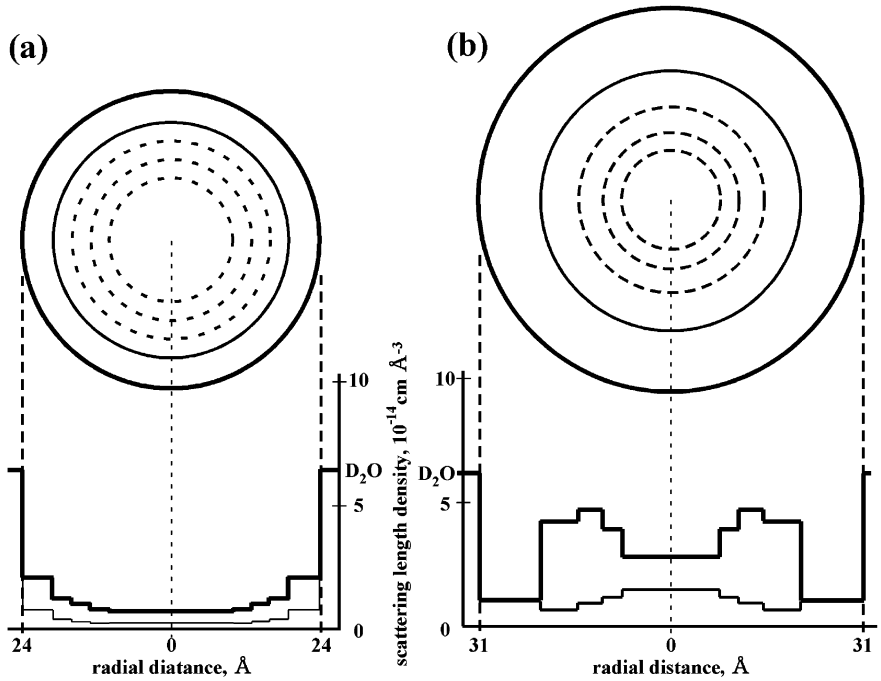

Figure 9. Layer geometry (upper) and coherent neutron scattering length density profile (lower) of G5 dendrimers as a function of the radial distance from a concentric center. (a) OH type PTMIN/AMAM dendrimer; (b) sugar ball. Thick and thin solid lines represent the scattering length densities of the segments in the dendrimers with and without penetrated solvents, ρ_i and $\rho_{\mathrm{den},i}$, respectively.

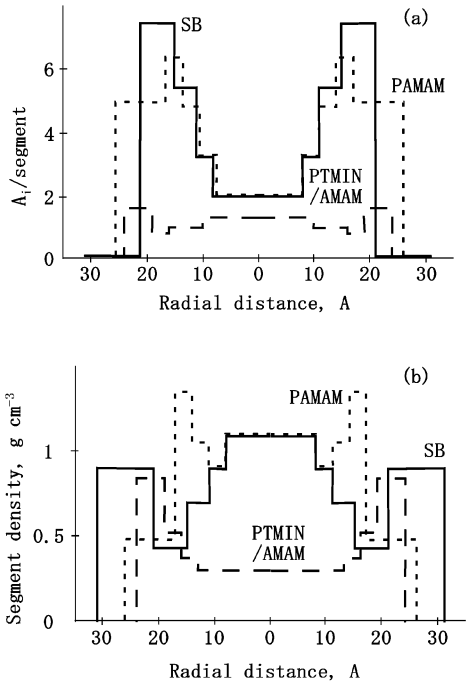

Figure 10. Water penetration (a) and segment density (b) into G5 dendrimers as a function of radial distance from a concentric center. Broken line, OH type PTMIN/AMAM dendrimer; solid line, sugar ball (SB); dotted line, OH type PAMAM dendrimer.

trated near the periphery.[13] This location of terminal groups agrees with the cases of the OH type PTMIN/AMAM dendrimer and the sugar ball. However, the minimum in segment density obtained for the sugar ball and the complicated density profile for the OH type PAMAM dendrimer have never been reported. In other words, theories and experiments, which have been reported before, do not satisfactorily explain the density profiles of all of the water soluble dendrimers obtained in the present work. This indicates that the chemical structures of the interior and exterior units are strongly correlated with the density profiles.

Conclusions

OH type PTMIN/AMAM dendrimers and sugar balls, which are layer−block dendrimers with different interior and exterior chemical structures, were investigated by AFM, TEM, DLS, and SANS. Their sizes were determined and compared with that of OH type PAMAM dendrimers. The apparent radii R_G calculated from the Guinier region in SANS depend on the D_2O content (% D_2O) in the mixed solvent D_2O-H_2O. This indicates that there is a segment distribution in the dendrimer. Then, the segment density and the solvent penetration were evaluated by the analysis of SANS results, using a five layers model.

The segment density profiles of the dendrimers reported in the present work do not necessarily agree with the theoretical expectations and experimental results reported before.[11,13,14,16] This suggests that the segment density profile depends on the interior and exterior chemical structures of dendrimers, that is, on the spatial size of the segment units and the nature of the functional groups in the dendrimers.

Acknowledgment. We are grateful to Drs. T. Otomo, S. Shimizu, and T. Adachi at KEK for their help on the SANS measurements. The experiments at JRR-3 were done under the approval of the Neutron Scattering Program Advisory Committee (Proposal Nos. 99-050 and 99-194).

References and Notes

(1) (a) Tomalia, D. A.; Baker, H.; Dewald, J.; Hall, M.; Kallos, G.; Martin, S.; Roeck, J.; Ryder, J.; Smith, P. *Polym. J.* **1985**, *17*, 117. (b) Tomalia, D. A.; Naylor, A. M.; Coddard, W. A., III. *Angew. Chem. Int. Ed. Engl.* **1990**, *29*, 138.

(2) (a) Frechét, J. M. J. *Science* **1994**, *263*, 1710. (b) Frechét, J. M. J.; Henmi, M.; Gitsov, I.; Aoshima, S.; Leduc, M. R.; Grubbs, R. B. *Science* **1995**, *269*, 1080.

(3) Bauer, B.; Briber, R. M.; Hammouda, B.; Tomalia, D. A. *Polym. Mater. Sci. Eng.* **1992**, *66*, 428.
(4) Briber, R. M.; Bauer, B. J.; Hammouda, B.; Tomalia, D. A. *Polym. Mater. Sci. Eng.* **1992**, *66*, 430.
(5) Scherrenberg, R.; Coussens, B.; van Vliet, P.; Edouard, G.; Brackman, J.; de Brabander, E. *Macromolecules* **1998**, *31*, 456.
(6) Ramzi, A.; Scherrenberg, R.; Brackman, J.; Joosten, J.; Mortensen, K. *Macromolecules* **1998**, *31*, 1621.
(7) Stark, B.; Stühn, B.; Frey, H.; Lach, C.; Lorenz, K.; Frick, B. *Macromolecules* **1998**, *31*, 5415.
(8) Nisato, G.; Ivkov, R.; Amis, E. J. *Macromolecules* **1999**, *32*, 5895.
(9) Nisato, G.; Ivkov, R.; Amis, E. J. *Macromolecules* **2000**, *33*, 4172.
(10) Evmenenko, G.; Bauer, B. J.; Kleppinger, R.; Forier, B.; Dehaen, W.; Amis, E. J.; Mischenko, N.; Reynaers, H. *Macromol. Chem. Phys.* **2001**, *202*, 891.
(11) Pötschke, D.; Ballauff, M.; Lindner, P.; Fischer, M.; Vögtle, F. *Macromolecules* **1999**, *32*, 4079.
(12) Imae, T.; Funayama, K.; Aoi, K.; Tsutsumiuchi, K.; Okada, M.; Furusaka, M. *Langmuir* **1999**, *15*, 4076.
(13) Topp, A.; Bauer, B. J.; Klimash, J. W.; Spindler, R.; Tomalia, D. A.; Amis, E. J. *Macromolecules* **1999**, *32*, 7226.
(14) de Gennes, P. G.; Hervet, H. *J. Phys. Lett.* **1983**, *44*, L-351.
(15) Naylor, A. M.; Goddard, W. A., III; Kiefer, G. E.; Tomalia, D. A. *J. Am. Chem. Soc.* **1989**, *111*, 2339.
(16) Lescanec, R. L.; Muthukumar, M. *Macromolecules* **1990**, *23*, 2280.
(17) Boris, D.; Rubinstein, M. *Macromolecules* **1996**, *29*, 7251.
(18) Welch, P.; Muthukumar, M. *Macromolecules* **1998**, *31*, 5892.
(19) Lue, L. *Macromolecules* **2000**, *33*, 2266.
(20) Ganazzoli, F.; Ferla, R. L.; Terragni, G. *Macromolecules* **2000**, *33*, 6611.
(21) Aoi, K.; Tsutsumiuchi, K.; Yamamoto, A.; Okada, M. *Tetrahedron* **1997**, *53*, 15415.
(22) Aoi, K.; Tsutsumiuchi, K.; Yamamoto, A.; Okada, M. *Macromol. Rapid Commun.* **1998**, *19*, 5.
(23) Tsutsumiuchi, K.; Aoi, K.; Okada, M. *Polym. J.* **1999**, *31*, 935.
(24) Guinier, A.; Fournet, G. *Small-Angle Scattering of X-rays*; Wiley: New York, 1955.
(25) Glatter, O.; Kratky, O. *Small-Angle X-ray Scattering*; Academic Press: London, 1982.
(26) Chen, S. H. *Annu. Rev. Phys. Chem.* **1986**, *37*, 351.
(27) Chen, S. H.; Lin, T. L. *Methods Exp. Phys.* **1987**, *23*, 489.
(28) Feigin, L. A.; Svergun, D. I. *Structure Analysis by Small-Angle X-ray and Neutron Scattering*; Taylor, G. W., Ed.; Plenum: New York, 1987.
(29) Lindner, P.; Zemb., Th. *Neutron, X-ray and Light Scattering: Introduction to an Investigative Tool for Colloidal and Polymeric Systems*; North-Holland: Amsterdam, 1991.
(30) Chen, S. H.; Bendedouch, D. *Methods in Enzymology*; Hirs, C. H. W., Timasheff, S. N., Eds.; Academic Press: New York, 1986; pp 130, 79.
(31) Stuhrmann, H. B.; Fuess, H. *Acta Crystallogr.* **1976**, *A32*, 67.
(32) Jacrot, B. *Rep. Prog. Phys.* **1976**, *39*, 911.
(33) Stuhrmann, H. B.; Miller, A. *J. Appl. Crystallogr.* **1978**, *11*, 325.
(34) Funayama, K.; Imae, T. *J. Phys. Chem. Solid* **1999**, *60*, 1355.